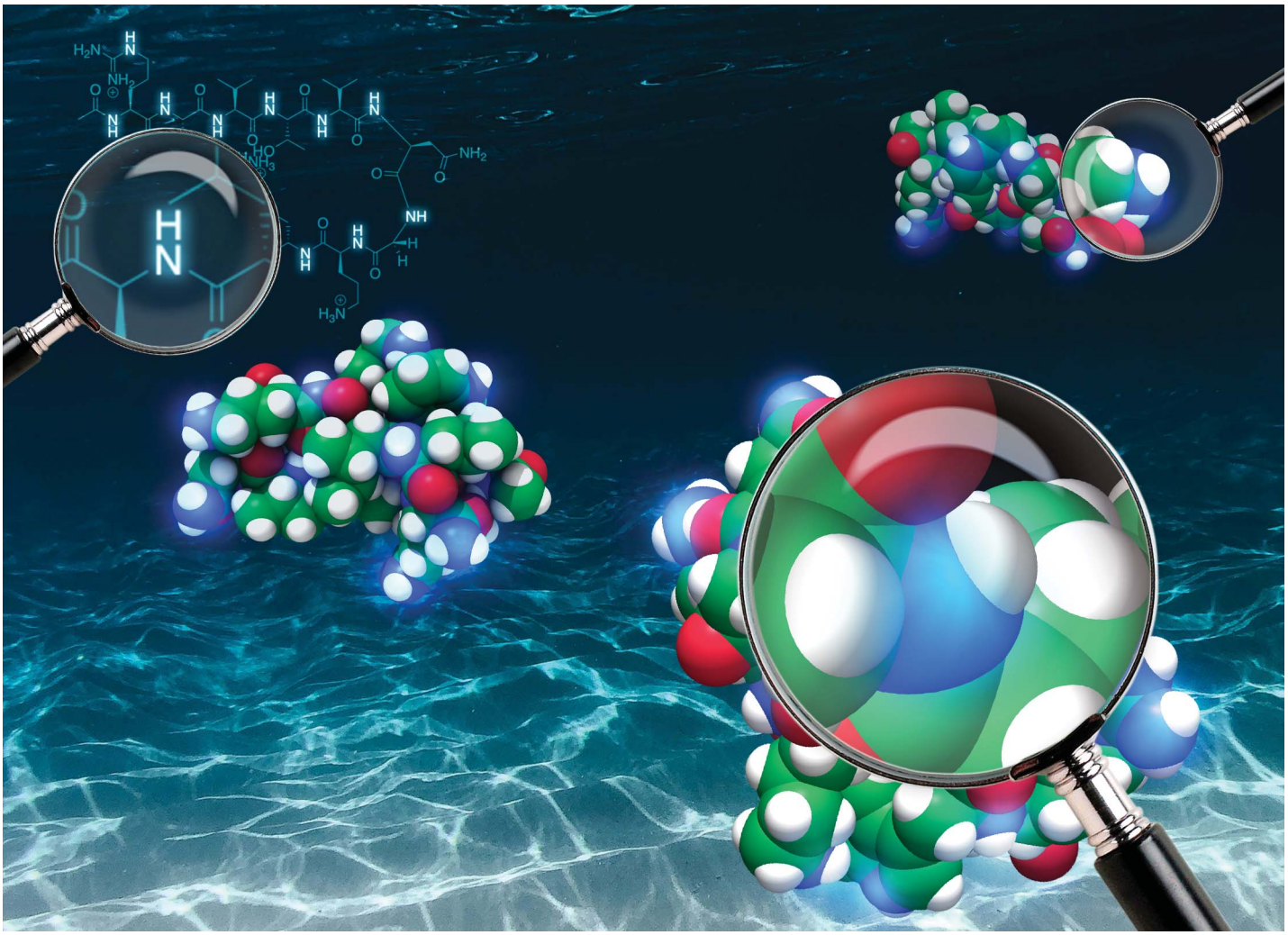

Showcasing research from Professor Bruce C. Gibb's laboratory, Department of Chemistry, Tulane University, New Orleans, Louisiana, USA.

Probing the non-covalent forces key to the thermodynamics of β-hairpin unfolding

Local reporting, i.e. monitoring all the mainchain amides of folded β-hairpin peptides, can provide a wealth of thermodynamic information about the non-covalent interactions within folded proteinaceous structures.

As featured in:

See Bruce C. Gibb *et al.*, *Chem. Sci.*, 2024, **15**, 15588.

ROYAL SOCIETY OF CHEMISTRY

rsc.li/chemical-science

Registered charity number: 207890

Chemical Science

ROYAL SOCIETY OF CHEMISTRY

EDGE ARTICLE

View Article Online
View Journal | View Issue

Cite this: *Chem. Sci.*, 2024, **15**, 15588

All publication charges for this article have been paid for by the Royal Society of Chemistry

Probing the non-covalent forces key to the thermodynamics of β-hairpin unfolding†

Thien H. Tran, [a] Priyanka Prusty, [a] Meghan Ricciardi, [b] Christopher R. Travis, [b] Marcey L. Waters [b] and Bruce C. Gibb [*a]

Received 27th May 2024
Accepted 24th August 2024

DOI: 10.1039/d4sc03464c

rsc.li/chemical-science

Although it is well understood that the graph of the free energy of unfolding (Δ*G*) of a globular protein with temperature approximates to a negative parabola, there is as yet no link between this global (G) $\Delta G_G(T)$ function and the individual structural elements—residue type and the non-covalent forces between groups—contributing to it. As such, there is little understanding of how each structural element contributes to the globally assessed changes of enthalpy (ΔH_G), entropy (ΔS_G), and heat capacity ($\Delta C_{p(G)}$) of unfolding calculated from the $\Delta G_G(T)$ function. To address this situation, we consider here an alternative approach to examining fold stability. Specifically, we examine the local (L) reporting of the thermodynamics of unfolding provided by each residue. By using ^{1}H NMR spectroscopy to monitor the response of the individual mainchain amide N–H groups of β-hairpin peptides with temperature, we generate local $\Delta G_L(T)$ functions, using these to calculate the local enthalpy (ΔH_L), entropy (ΔS_L), and heat capacity ($\Delta C_{p(L)}$) of unfolding. Mapping the thermodynamic changes in this way, for specific point-mutations, provides new information about how specific residues, non-covalent forces, and secondary structure type, contribute to folding. This type of information provides new details of the factors contributing to the typically measured global $\Delta G_G(T)$ function.

Introduction

The multi-billion-dollar biologics market[1,2] is reliant on the stability of the biomacromolecular components during manufacture, storage, and transport. Beyond formulation control with osmolytes and salts, temperature control protocols such as those involving freeze/thaw cycles are key considerations to maintaining activity. This last point is intimately linked to the phenomenon of cold denaturation, whereby folded proteins exhibit a temperature of maximum stability (T_{max}) from which both increasing and decreasing the temperature leads to unfolding. Whereas heat denaturation of proteins is intuitive, cold denaturation[3–25] is less so; a lowering of the temperature below T_{max} induces the protein to release heat and become more disordered.

Despite substantial effort, there are many open questions surrounding cold denaturation, and the parabolic nature of the free energy of unfolding with temperature ($\Delta G_u(T)$) function in general. The $\Delta G_u(T)$ function is probed using a combination of the two-state model and the Gibbs–Helmholtz equation (eqn (1)) relating it to changes in enthalpy (ΔH°_u), entropy (ΔS°_u), and heat capacity (ΔC°_p) of unfolding. Here, the positive ΔC°_p typically observed with protein unfolding, leads to $\Delta G_u(T)$ approximating to a negative parabola, with ΔC°_p defining the curvature and ΔS°_u and ΔH°_u defining its position on the *x*- and *y*-axes respectively. The maximum of the parabola, T_{max}, is controlled by ΔC°_p and $\Delta S^\circ_u (T_{max} = 298 \times e^{-\Delta S^\circ_u/\Delta C^\circ_p})$, and it follows from $S = -dG/dT$ that $\Delta S^\circ_u = 0$ at T_{max}, *i.e.*, the (un)folding process at T_{max} is entirely driven by enthalpy.[26]

$$\Delta G_u(T) = \left(\Delta H^\circ_{u,\,298\ K} + \Delta C^\circ_{p,u}(T - 298)\right) - T\left(\Delta S^\circ_{u,298\ K} + \Delta C^\circ_{p,u}\ln(T/298)\right) \quad (1)$$

Normally, techniques such as circular dichroism (CD) spectroscopy are used to assess the global (G) stability with temperature: $\Delta G_G(T)$, and hence determine the globally defined enthalpy (ΔH_G), entropy (ΔS_G), and heat capacity ($\Delta C_{p(G)}$) of unfolding. However, this approach cannot explain why the $\Delta G_G(T)$ for metmyoglobin and ribonuclease A are very different;[27] the T_{max} value of the former approaches 40 °C, whereas that of ribonuclease A is well below 0 °C. In other words, there is a disconnect between protein structure, and the nature of the $\Delta G_G(T)$ parabola. In general terms, it is understood from small molecule studies[10,28–32] and large proteins[3–10,33] that a positive ΔC°_p is characteristic of non-polar groups being solvated upon unfolding, and that ΔC°_p is proportional to the

[a]*Department of Chemistry, Tulane University School of Science and Engineering, New Orleans, LA 70118, USA. E-mail: bgibb@tulane.edu*

[b]*Department of Chemistry, University of North Carolina at Chapel Hill, Chapel Hill, NC 27599, USA*

† Electronic supplementary information (ESI) available. See DOI: https://doi.org/10.1039/d4sc03464c

non-polar surface area.[34] On the other hand, polar residues are assumed to contribute lower or negative ΔC_p° values. However, beyond these generalities it is unclear how particular residues, secondary-structure type, or the multitude of non-covalent interactions (NCIs) within a folded structure contribute to the $\Delta G_G(T)$ parabola.[6,13–16,35–39] This situation is unfortunately made more complicated by the relatively high freezing point of water that—despite workarounds using supercooled solutions[40,41] reverse micelles,[19,21,42] organic[43] or mixed solvents,[44–46] osmolytes or denaturants,[39,47] or high pressure,[18,48,49]—can severely limit analysis. New approaches are therefore needed to forge a stronger link between structure and the $\Delta G_G(T)$ function, and hence improve our understanding of biologics stability and the properties of proteins in general.

As an alternative to the normal approaches, here we investigate the stability of β-hairpin peptides using each individual mainchain amide N–Hs as a reporter. Thus, we utilize ^{1}H NMR spectroscopy to map the local (L) $\Delta G_L(T)$ responses of each amide signal, and so obtain the local ΔH_L, ΔS_L, $\Delta C_{p(L)}$ and $T_{max(L)}$ value as reported by each residue. Thus, our approach uses the two-state model to treat each residue as a unique, uncoupled system fully independent of the other residues. This approach is of course incongruous with the fact that the non-covalent interactions between residues dictate that they do not act independently, but are coupled. Nevertheless, as we discuss this per-residue analysis does reveal new details of the individual contributions from each, the non-covalent interactions between them, as well as trends in the thermodynamic parameters that shed light on how β-sheet and β-turns contribute to (un)folding and hence the form of $\Delta G_G(T)$ parabolae. As such, this approach amounts to a first step towards a new model relating individual residue contributions to global protein stability.

Results

The structures of the β-hairpins used are shown in Fig. 1 (see Section 1 of the ESI for synthetic details†). Their general design originated in the Gellman group,[50–52] but included two modifications from the Waters' lab;[37,53–55] specifically, a tyrosine to

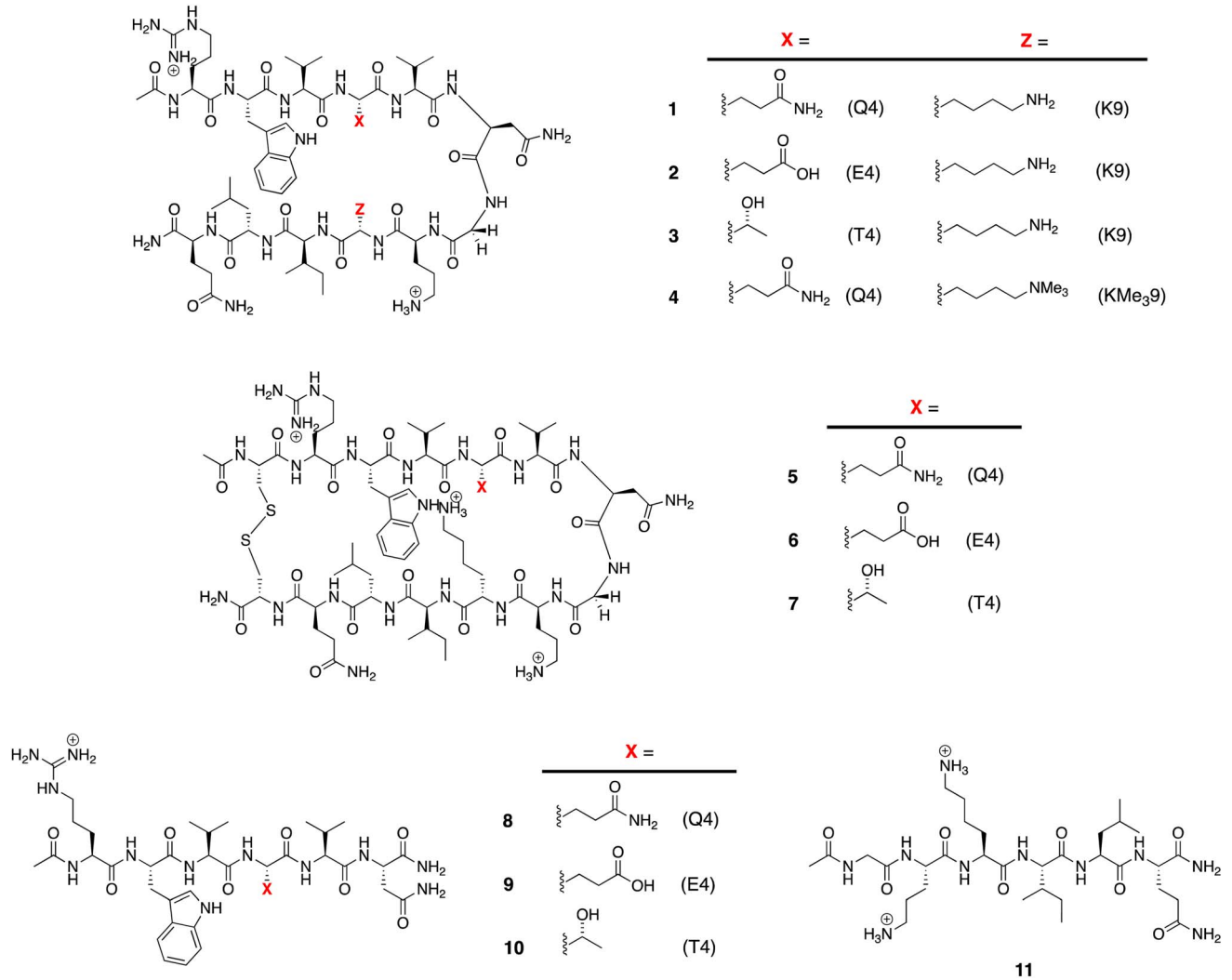

Fig. 1 Peptides used in this study.

tryptophan (Y2W) mutation to give an enhanced W2···Z9 cation–π interaction, and a proline to asparagine (P6N) mutation to give a $_5$VNGO$_8$ (O = ornithine, Orn) type 1′ turn.[56,57] Thus, these β-hairpins are designed to be held together by a core formed of a cation–π interaction between W2 and X9 (Lys-9 (K9) or trimethyl Lys-9 (KMe$_3$9)), and non-polar interactions between W2 and leucine-11 (L11), and valine-3 (V3), V5, and isoleucine-10 (I10).

Following literature precedent, ^{1}H NMR spectroscopy was first used to determine the extent of global folding by measuring the signal separation of the C$_\alpha$H protons of glycine-7 (G7).[37,58] By comparison to macrocycles **5–7** as surrogates for the fully-folded state, and half-peptides **8–11** as surrogates for the unfolded state, G7 can be used as a global reporter of peptide-folding *via* eqn (2):

$$\text{Fraction folded } (f) = [\delta_{obs} - \delta_0]/[\delta_{100} - \delta_0] \quad (2)$$

where δ_{obs} is the observed G7 signal split of the C$_\alpha$H protons (in ppm) of the hairpin, and δ_{100} and δ_0 are respectively the signal differences in the corresponding (100% folded) macrocyclic surrogate and (0% folded) 6-mer peptides. By this approach, β-hairpins **1–4** were determined to be respectively 52%, 77% 79% and 78% folded at room temperature (Section 4, ESI†). Thus, each of the three, single-point mutations upon peptide **1**, to give **2**, **3**, or **4**, increased the folding percentage by ∼26%. Fraction folded values (*f*) can be readily converted to the global free energy of unfolding ΔG_G using eqn (3). These values are given in Table 1.[59]

$$\Delta G_G = -RT\ln((1 - f)/f) \quad (3)$$

To determine the remaining thermodynamic parameters, we monitored the G7 C$_\alpha$H protons signal-splitting from 10 to 60 °C. This data (Section 4, ESI†) was then fitted to the Gibbs–Helmholtz equation (eqn (1)) to yield the complete, thermodynamic profile of unfolding (Table 1).[60] This global analysis revealed similar endothermicities for unfolding **1**, **2** and **4**, but a much larger endothermicity of unfolding of **3**. Additionally, each unfolding process was entropically promoted and involved positive $\Delta C_{p(L)}$ values attributed to the hydration of non-polar groups upon unfolding.[10]

The majority of work with hairpins involve pH values ∼ 7, where amide N–H exchange rates are close to the NMR timescale and their signals not always observable. Consequently, to observe each mainchain amide N–H signal we carried out all studies at pH = 2.3.[61] Full experimental details are provided in the ESI.†

Tracking the mainchain N–H amide signals of each peptide as a function of temperature ($\delta(T)$) resulted in twelve curves for each peptide, which were classified in three ways (Fig. 2): data that is approximately linear with a positive gradient (blue), data that is approximately linear and possessing a negative gradient (green), and data this is distinctly non-monotonic (red). Although this is $\delta(T)$ data rather than $\Delta G_L(T)$ data, several points are worthy of note. First, the blue functions arises largely from outward-pointing amide groups. The two exceptions are the N-terminal R1 amide that is least likely to be involved in inter-strand hydrogen bonding, and the O8 amide involved in a weak, non-linear hydrogen bond because of its tight proximity to the turn and high solvation. Due to a lack of curvature, this data suggests a low $\Delta C_{p(L)}$ and a high $T_{max(L)}$. Second, the N6 signal function (green) suggests a low $\Delta C_{p(L)}$ and a low $T_{max(L)}$. Asn-6 is generally considered to be an unusual residue because of its extreme down-field position and its sensitivity to folding/unfolding; hence the negative gradient. Third, the non-monotonic functions (red) are all from strongly hydrogen bonded amides intimately associated with the cation–π–hydrophobe core of the peptide. These have observable (or close to observable) δ_{max} values, and suggest relatively high $\Delta C_{p(L)}$ values. As we discuss below, these three assessments on $\Delta C_{p(L)}$ residue values large hold when the thermodynamic data is calculated.

Separately, a comparison of the response of each residue in the four peptides demonstrates that the Q4T mutation (**1** → **3**) is intrinsically different from the other mutations. Thus, the $\delta(T)$ response of the X4 residue in **1** and **3** are very different, whereas the differences in the responses of X4 in **1** and **2** are quite similar (and the difference in the response of X9 in **1** and **4** essentially the same).[62] Moreover, relative to the other mutations, the T4 residue in **3** induces non-monotonicity in the data of two additional residues: outward pointing W2 and K9.

Using the corresponding reference peptides and eqn (1) and (3), we determined the local (L) $\Delta G_L(T)$ curves and calculated the thermodynamics of unfolding reported by each residue.[63] Fig. 3 shows this ΔH_L ΔS_L and $\Delta C_{p(L)}$ data for the reporting residues, as well as their calculated $T_{max(L)}$ values. *En masse*, the ΔH_L and ΔS_L data is complex, but the $\Delta C_{p(L)}$ data does reveal that the

Table 1 Room temperature (298 K), global (G) thermodynamic parameters of unfolding of peptides **1–4** as reported by G7[a,b]

Thermodynamic parameters	1	2	3	4
ΔG_G (kJ mol^{-1})	0.20 (0.02)	3.04 (0.52)	3.28 (0.36)	3.14 (0.41)
ΔH_G (kJ mol^{-1})	12.76 (0.51)	12.95 (1.83)	20.88 (0.29)	13.64 (1.78)
ΔS_G (J mol^{-1} K^{-1})	42.47 (1.73)	33.03 (6.16)	59.55 (0.97)	35.03 (6.01)
$\Delta C_{p(L)}$ (J mol^{-1} K^{-1})	554.3 (43.8)	677.4 (156.4)	414.8 (24.6)	543.6 (27.1)
$T_{max(G)}$ (K)	276 (2)	284 (4)	258 (2)	279 (3)

[a] Errors are shown in parenthesis, and are determined by: error propagation using eqn (1) and (2) (ΔG_G), and fitting to eqn (3) (ΔH_G, ΔS_G, and $\Delta C_{p(L)}$). [b] The data for peptide **2** and **4** was similar to that obtained previously by the same approach.[38,53,55]

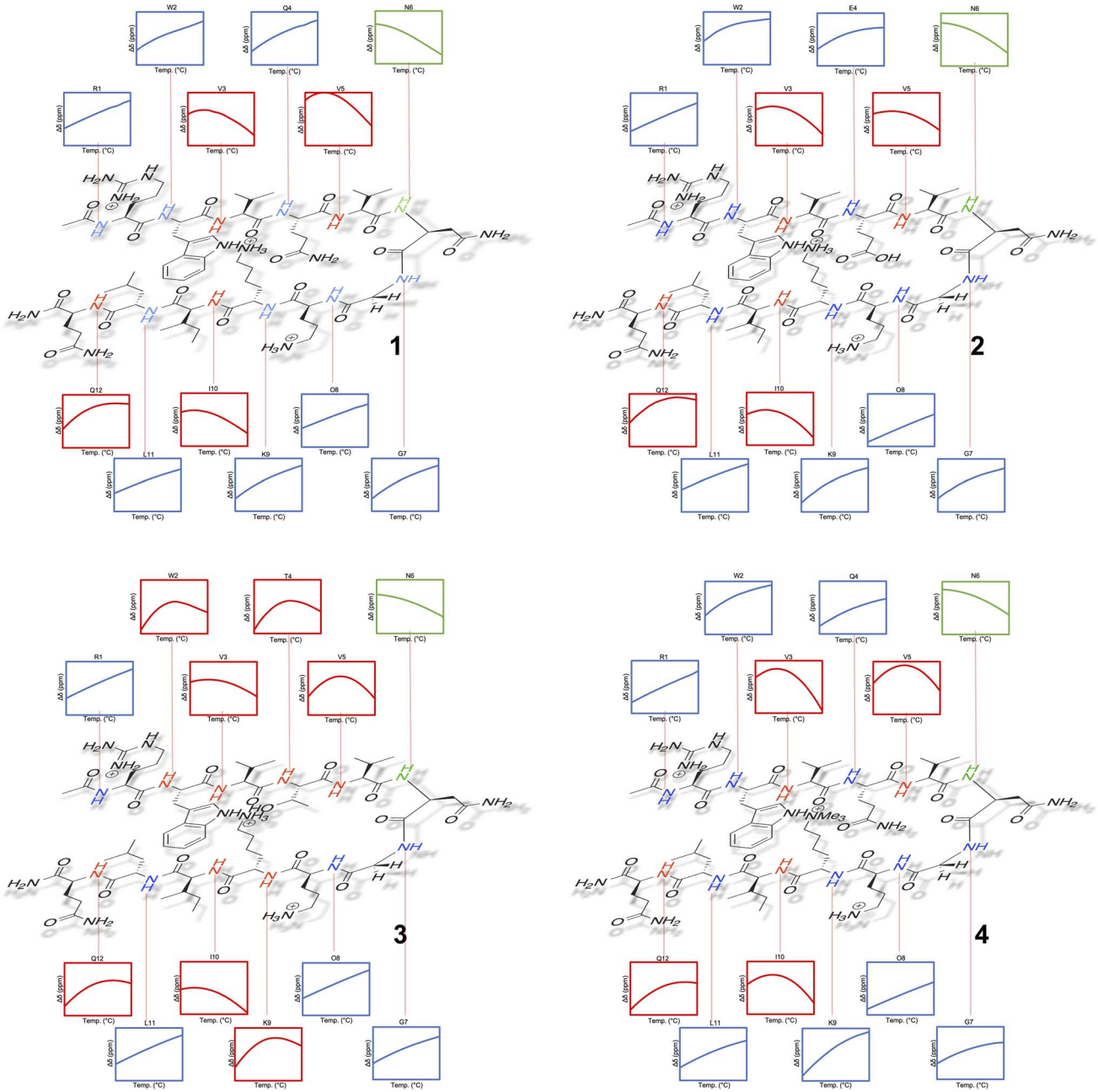

Fig. 2 Temperature dependent ^{1}H NMR signal shifts (δ) for each individual mainchain amide N–H group of peptide **1–4**. For each box of data, the height of the y-axis is 0.3 ppm (normalized scale, δ at 298 $K = 0$), and the width along the x-axis is 10–60 °C (283–333 K). Shown functions are the average obtained from the triplication of data.

smallest heat capacity changes are reported by the turn residues $_6$NGO$_8$, consistent with their relatively high degree of solvation in the folded state. The $\Delta C_{p(L)}$ data also reveals remarkably high values for Z9. As (similarly-cationic) O8 does not show such extreme values, we assume this is intrinsic to the W2···Z9 cation–π interaction. Between these extremes are values reported by Q12, W2, and the non-polar residues in the core. Separately, the $T_{max(L)}$ data reveals that turn residues have generally lower values than those toward the termini.

In the following discussion, we will refer to the data shown in Fig. 3 periodically. However, analyzing this data by considering the changes upon each point-mutation of **1** provides more insight, and we represent the per-residue differences between the two peptides using the 'bubble maps' shown in Fig. 4. Each row in Fig. 4 shows the percentage change in ΔH_L, ΔS_L, and $\Delta C_{p(L)}$, as well as the calculated $T_{max(L)}$ changes reported by each residue, for the mutations: Q4E (**1** → **2**), Q4T (**1** → **3**), and K9KMe$_3$ (**1** → **4**).

In the Q4E mutation, the enthalpy map demonstrates the increased folding percentage (globally, 52 to 77% folded) is largely driven by the turn residues, where all residues report an increased endothermicity of unfolding. In contrast, despite the

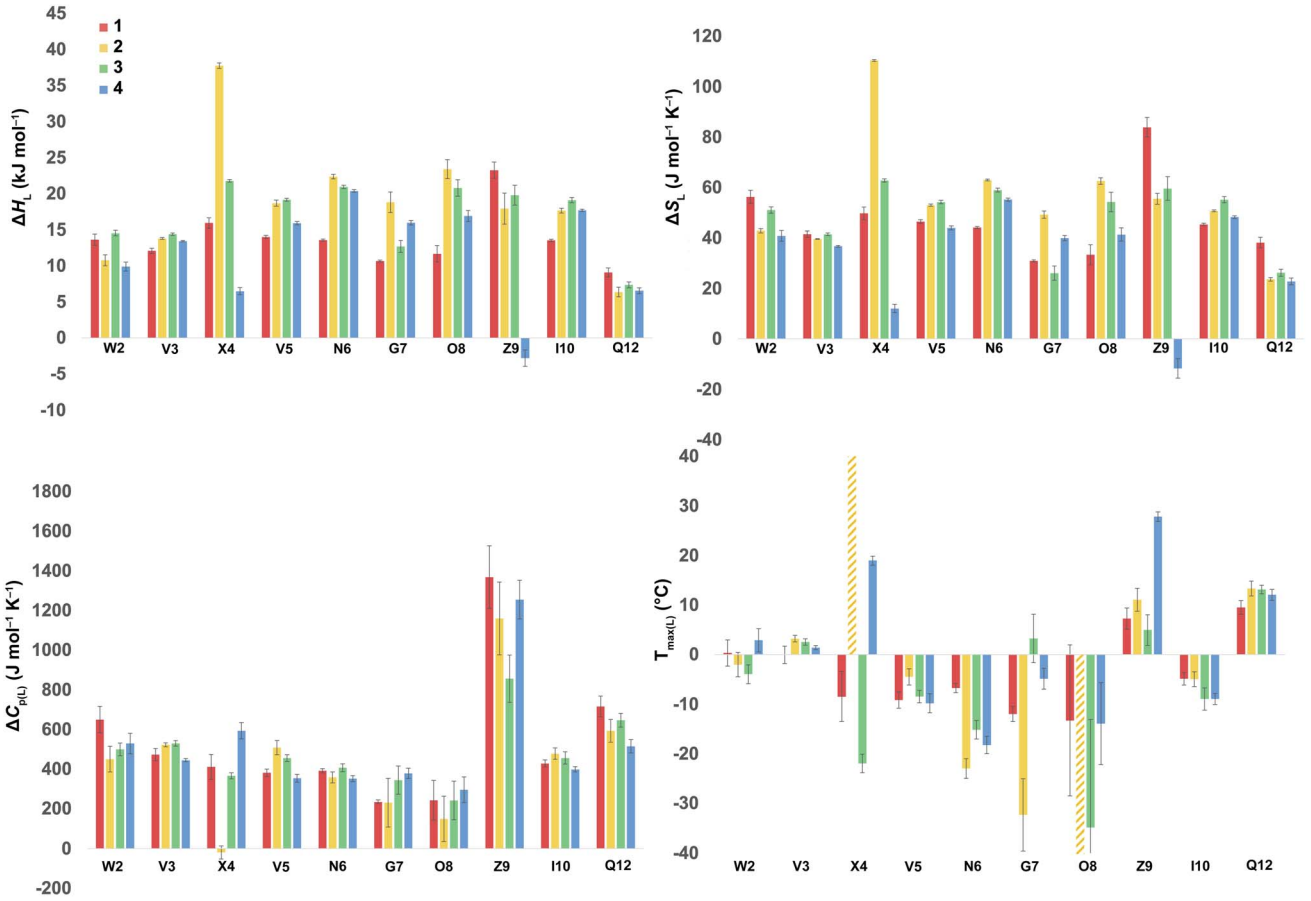

Fig. 3 ΔH_L, ΔS_L, and $\Delta C_{p(L)}$ of unfolding and $T_{max(L)}$ values as reported by each residue of peptides **1**–**4**. Values are derived from the ^{1}H NMR signal shift, for each individual mainchain amide N–H group, as a function of temperature (using eqn (1)–(3)). Because of signal overlap between each peptide and its reference 6-mer half peptide, data could not be obtained for R1 and L11. Extreme changes in $T_{max(L)}$ for residues X4 (very high) and O8 (−77 °C) in **2** are cut off and highlighted with hatched color. Shown error bars are fitting errors.

lack of data from R1 and L11, the enthalpic contributions from the terminal "half" of the peptide are small. The largest change is observed for X4. As Fig. 3 shows, the E4 residue of **2** is quite distinctive in the magnitude of the reported endothermicity of unfolding. Modeling suggests that the E4 carboxylic acid carbonyl can readily form a hydrogen bond to the G7 amide N–H (Section 2.3, ESI†); an extra non-covalent interaction supported by the downfield shift of the proton upon the Q4E mutation. We assume this additional non-covalent interaction is a major contributor to the enhanced stability of **2**. In contrast, conspicuous in its absence upon the Q4E mutation is a sizeable change in the enthalpy change reported by K9. This suggests that the mutation has little effect on any X4···K9 ion–dipole interaction (–NH^{3+}···O=C), or despite the low pH, the presence of a salt-bridge in peptide **2**. Indeed, the only observable NOEs involving the sidechain methylenes of E4 are with the amides of V5, G7, and O8.[64] Taken together, this data is consistent with a E4···G7 hydrogen bond in **2** that augments the extent of global folding.

The entropy bubble map reveals that, without exception, all residues report enthalpy–entropy compensation (see Section 5.2 of ESI†). In other words, the tighter fold of the Q4E mutation results in the majority of the increased ordering of the system occurring at the turn.

Examining the heat capacity map reveals a significant change at the mutation site. The specific $\Delta C_{p(L)}$ values for X4 of **1** and **2**, are +412 and −19 J mol^{-1} K^{-1} (Fig. 3) confirm a surprising large change in the reported $\Delta C_{p(L)}$ upon the minor change of replacing the –C(O)NH$_2$ of **1** with a –C(O)OH in **2**. As there is no evidence of a meaningful E4···K9 interaction, we tentatively attribute the low $\Delta C_{p(L)}$ value of E4 in **2** to its hydrogen bond to the amide of G7. However, solvation changes may also play a role here.

For more information concerning the heat capacity differences between X4 of **1** and **2**, we compared the $\Delta C_{p(L)}$ values reported by each residue of each peptide (Fig. 3) to the partial molar heat capacity change of hydration of the amino acid sidechains ($\Delta_g^w C_p$) calculated by Privalov.[65] Subtraction of the $\Delta_g^w C_p$ values from the data given in Fig. 3 reveals the excess heat capacity $\Delta C_{p(excess)}$ within each residue in each folded peptide.[66] Fig. 5 shows this data. Focusing on the data for X4, whereas the Q4 residue of **1** reports a positive $\Delta C_{p(excess)}$ suggesting that this residue is poorly solvated in the folded state, the E4 residue of **2** reports a negative $\Delta C_{p(excess)}$. Since $\Delta_g^w C_p$ corresponds to the

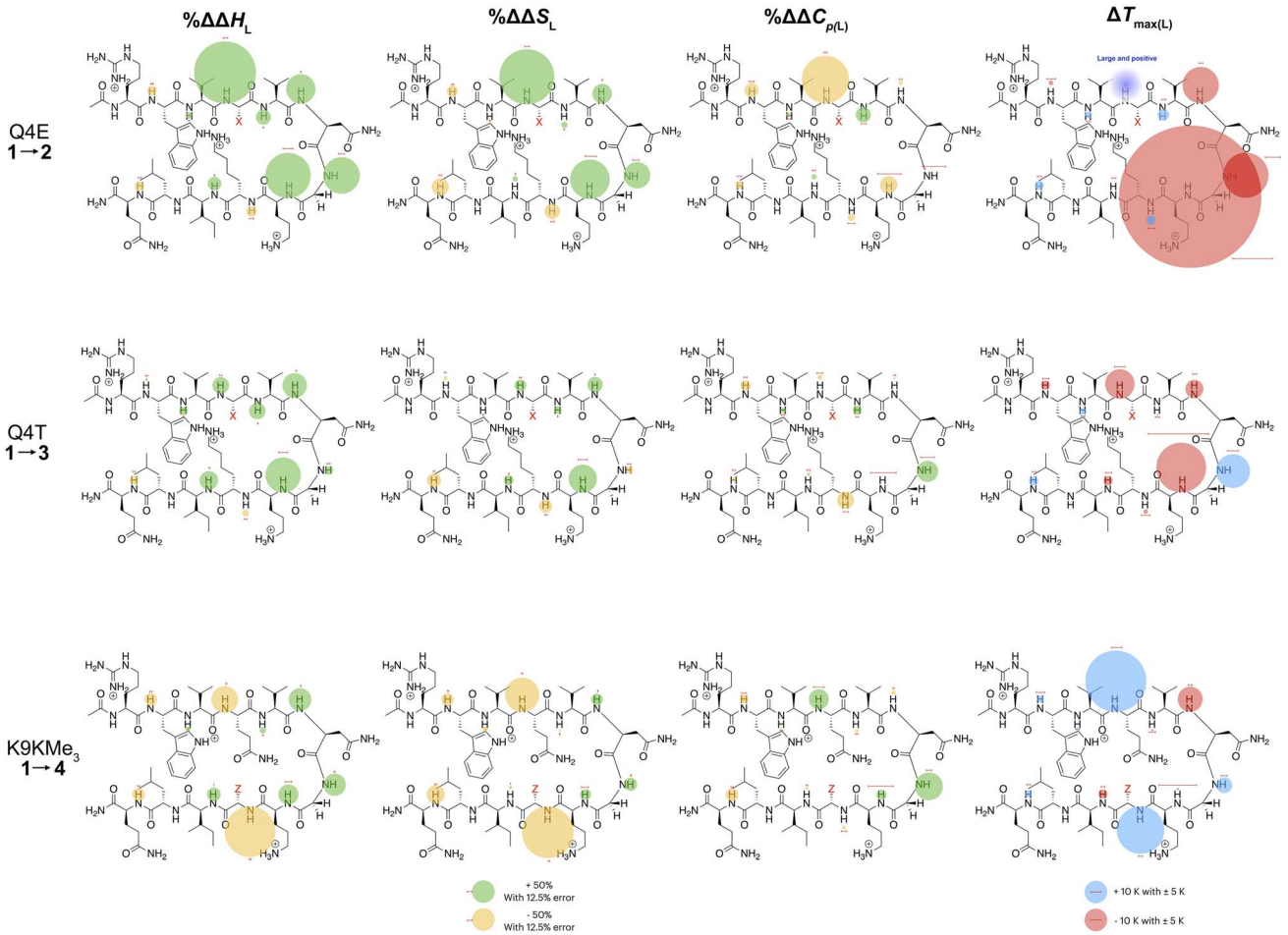

Fig. 4 Per-residue reporting of the % $\Delta\Delta H_L$, % $\Delta\Delta S_L$ and % $\Delta\Delta C_{p(L)}$ and $\Delta T_{max(L)}$ for unfolding of the mutations: top row, Q4E (**1** → **2**); middle row, Q4T (**1** → **3**), and; bottom row, K9KMe$_3$ (**1** → **4**). Because of signal overlap between each peptide and its reference 6-mer half peptide, data could not be obtained for R1 and L11. For the ΔH_L, ΔS_L and $\Delta C_{p(L)}$ data, changes are shown as percentage increases (green) or decreases (yellow) proportional to the area of the bubble. For $\Delta T_{max(L)}$, changes are shown in kelvin (K). All values are indicated, though bubbles for insignificant changes may not be apparent. Scaling bubbles and error bars for the two types of bubbles are shown at the foot of the figure. Specific values of ΔH_L, ΔS_L and $\Delta C_{p(L)}$ as reported by each amide N–H are given in Fig. 3.

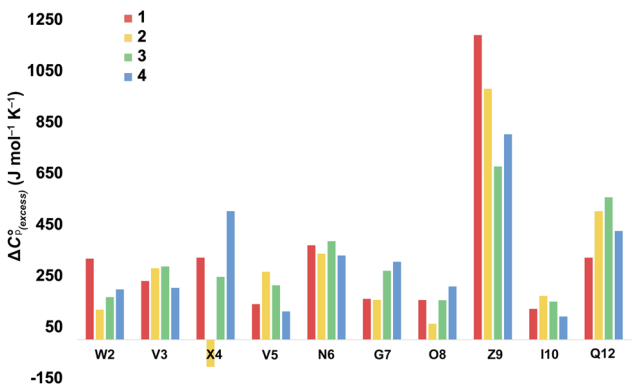

Fig. 5 Excess heat capacity $\Delta C_{p(excess)}$ reported by each residue. The shown values are differences between Privalov's calculated heat capacity change of hydration of amino-acid sidechains ($\Delta_g^w C_p$) and the $\Delta C_{p(L)}$ reported in Fig. 3.

fully solvated side chain, we attribute this negative $\Delta C_{p(excess)}$ to the hydrogen bonding between E4 with G7 acting as a strong heat sink that is lost upon the unfolding of **2**.

Other significant changes in $\Delta C_{p(L)}$ from the Q4E mutation (Fig. 4) occur at W2, V5, and O8. The increase at V5 and decrease at O8 may result from hydration changes induced respectively by the sidechain methylenes and terminal carboxylic acid of E4. In contrast, W2 is remote from E4, and so this change may simply reflect a subtle repacking of the core.

The $\Delta T_{max(L)}$ values for the Q4E mutation are shown in Fig. 4. Because E4 in **2** reports a very small $\Delta C_{p(L)}$ and a relatively large error, and because of the corresponding large increase in ΔS_L, the T_{max} reported by E4 is unreliable. However, the large increases in $T_{max(L)}$ for turn residues $_6$NGO$_8$ are significant, and are all rooted in the increased order (ΔS_L) of the turn. The value for O8 is especially large because in addition to the change in order, there is also an increase in local hydration ($\Delta C_{p(L)}$) upon hydrogen bonding of E4 to neighboring G7.[67]

For the Q4T mutation (**1** → **3**), the enthalpy map also demonstrates that the increased folding percentage (globally, 52 to 79% folded) is driven by the turn. These enthalpy changes are generally smaller than in the Q4E mutation. In the energy-minimized structure of **3** the T4 OH group hydrogen bonds to

the V3 carbonyl, whilst the T4 methyl fills the small concavity created by the turn residues (see Section 2.4 of ESI†) In contrast, in the structure of **2**, the E4 carboxylic acid hydrogen bonds to the G7 amide (Section 2.3, ESI†). The enthalpy bubble maps for the Q4E and Q4T mutations suggest that the E4···G7 hydrogen bond contributes more to folding than does the T4 sidechain interactions.

As with the Q4E mutation, the enthalpic contributions from the terminal "half" of the peptide are relatively small. Furthermore, the enthalpy and entropy bubble maps reveal that all residues—barring G7—report enthalpy–entropy compensation (see Section 5.2 of the ESI†).

Examining the $\Delta C_{p(L)}$ map for Q4T reveals only weak patterning. However, as with the Q4E mutation the inner-core amides of V3, V5, and I10 all report small increases in $\Delta C_{p(L)}$, suggesting that these protons are more isolated from water in **2** and **3** than they are in **1**. The excess heat capacity values reported by these residues (Fig. 5) also support this notion. However, the biggest changes in heat capacity for the Q4T mutation are observed at G7 (47% increase from 234 to 344 J mol^{-1} K^{-1}) and K9 (37% decrease from 1369 to 858 J mol^{-1} K^{-1}).[68] In hydrogen bonding to the V3 carbonyl, the T4 OH group is located at the end of the groove between the indole of W2 and the sidechain of K9 (3.0 Å from the K9 C_β methylene). And as just discussed, the T4 methyl rests in the concavity of the turn (see Section 2.4 of ESI†). Thus, we attribute the increase reported by G7 to a degree of shielding provided by the proximal (3.2 Å) T4 methyl, and the decrease reported by K9 to the hydration of the W2–K9 groove by the OH group. Heat capacity changes elsewhere are minor. Thus, as with the Q4E mutation, the Q4T mutation is not felt by the $_1$RW$_2$ and $_{10}$ILQ$_{12}$ sections of the hairpin.

The largest decreases in $T_{max(L)}$ for the Q4T mutation (Fig. 4) are for X4, N6, and O8, which are all rooted in the increased structure (order) in more folded **3**, whilst the large increase in $T_{max(L)}$ for G7 is rooted in both its large increase in $\Delta C_{p(L)}$ and its decrease in the entropy of unfolding.

A similar analysis (Fig. 4) can be carried out for the K9KMe$_3$ mutation (**1** → **4**), which increases (global) folding from 52 to 78%. From the enthalpy map it is apparent that half the residues report increases in the endothermicity of unfolding, and half decreases. The largest decreases are reported by W2, Q4, and Z9. For Z9, the cation–π interaction switches from one that enthalpically disfavors unfolding in **1** (ΔH_L = 23.3 kJ mol^{-1}), to one that enthalpically promotes unfolding in **4** (ΔH_L = −2.8 kJ mol^{-1}). These values are in contrast to the global values reported by G7 (Table 1). The other large reductions in ΔH_L reported by W2 and Q4, suggesting a non-covalent network in **4** involving W2···Z9···Q4. This was not apparent in **1–3**, but presumably the large size of KMe$_3$ is key here. Counteracting these sizable destabilizations are four turn residues that, as is the case with the other mutations, all report enhanced endothermicities of unfolding.

The entropy data for the K9KMe$_3$ mutation again reveals good enthalpy–entropy compensation, with the largest change in ΔS_L reported by Z9. Thus, although the cation–π interaction becomes energetically repulsive in folded **4**, this is more than compensated for by this interaction being promoted by entropy. As reported in Table 1, global analysis suggests the entropic benefit for unfolding **4** is smaller than that of **1**, but this hides the actual entropic benefits of forming the W2···KMe$_3$9 interaction.

The corresponding heat capacity data for K9KMe$_3$ shows that the most significant differences are at Q4 and G7. The change in absolute value for $\Delta C_{p(L)}$ reported by Z9 (Fig. 3) is nullified by a large error, but despite this there is evidently a 'knock-on' effect at Q4, and in turn, G7. For each residue the increase in $\Delta C_{p(L)}$ is indicative of a less polar environment for the turn residues, which we interpret as the large and non-polar headgroup of KMe$_3$9 of **4** crowding neighboring Q4 and reducing the hydration of the turn.

The largest $\Delta T_{max(L)}$ values for the K9KMe$_3$ mutation are reported by Q4, N6, and Z9 (Fig. 4). The positive change at Q4 is the result of order (ΔS_L) and solvation ($\Delta C_{p(L)}$) changes, whilst the positive change at Z9 is rooted in entropy; as is the decrease in $T_{max(L)}$ for N6. Thus, the favorable entropy of the W2···KMe$_3$ interaction dominates the large $T_{max(L)}$ increases reported by Q4 and K9.

Discussion

Considering the data collectively, we envision two important questions. First, what do these local reported thermodynamic values tell us about the physical forces at play within β-hairpins? And second, how does local data relate to the global data typically measured? Regarding the first question, local reporting evidently provides thermodynamic information that ties in with structural information from NMR and computation. We envision that ultimately we will be able to identify what can be called, thermodynamic signatures; singular or multifactorial thermodynamic measures that are characteristic of structural elements such as residue types/functional groups, secondary structure type, or NCIs between residues. The work here has focused on just four peptides, and it is obvious that a much larger set of data is required before a comprehensive list of definitive thermodynamic signatures can be formulated. Nevertheless, the data in hand does suggest some specific thermodynamic signatures, and points to others that will need further studies to confirm.

Comparing all three mutations, an increase in folding percentage is rooted mostly in the enthalpy and entropy changes in the turn region $_4$XVNGO$_8$. In terms of enthalpy, the largest changes in the turn are seen in the Q4E mutation (**1** → **2**). Smaller enthalpic enhancements are seen for the Q4T mutation (**1** → **3**) and the K9KMe$_3$ mutation (**1** → **4**); though they are smaller and the changes in the latter are masked somewhat by the change in the thermodynamics of the cation–π interaction reported by W2 and X9. The details of these differences are rooted in the different ways that each mutation enhances stability: the E4 acid group of **2** can hydrogen bond to the G7 amide; the T4 sidechain of **3** is involved in hydrogen bonding to the V3 carbonyl and packing the concavity of the turn, whilst the K9KMe$_3$ mutation changes the nature of the cation···π interaction to one that is enthalpically repulsive but entropically attractive. Thus, the K9KMe$_3$ mutation leads to

a reported exothermicity of unfolding; the opposite recorded by synthetic hosts[69,70] designed to recognize KMe_3 residues in histone proteins.[38,53,55,71–73]

From the limited set of four peptides, the introduction of a carboxylic acid (Q4E) or trimethylammonium (K9KMe_3) group induces large changes in the enthalpy and entropy data reported by the mutation site itself; the corresponding effect of the Q4T mutation is small. Moreover, observed enthalpy/entropy changes in neighboring residues are more apparent with the Q4E or K9KMe_3 mutations. However, more information is needed to determine if, for example, the E4 residue of **2** affects the neighboring turn residues directly or indirectly *via* solvent mediation. Similarly, the enthalpy/entropy data for the single K9KMe_3 hints at an X4···Z9 interaction in **4**, but other examples are needed to explore such a cross-strand interaction. In summary, enthalpy changes for the mutations studied are most evident at the turn residues. There are specifics still to explore here, but generally the observed enthalpy–entropy compensation means that increased stability is reflected in greater ordering of the turn residues.

In terms of the heat capacity changes, the effect of each mutation is generally focused on the turn residues, although the Q4E and K9KMe_3 mutations also affect the X4 $(i-1)$ site. We ascribe this to local changes in solvation brought about by mutation. However, further mutants are required to understand the subtilties of the patterning of positive and negative changes in the values reported by the different residues. This stated, the $\Delta C_{p(excess)}$ values reported in Fig. 5 reveal that the majority of residues report a positive excess heat capacity. The most striking observation here is the large, positive $\Delta C_{p(excess)}$ reported by X9. Each cation–π interaction of Z9 residues reports as 'extremely hydrophobic', with $\Delta C_{p(excess)}$ values demonstrating that unfolding leads to a very large increase in the heat storage capabilities of an ammonium group as water molecules replace the indole ring of W2 upon unfolding. We currently therefore view this high $\Delta C_{p(L)}$ of the cation–π interaction as a (singular) thermodynamic signature of this familiar NCI. In contrast, neighboring O8 is well solvated in the folded state and there is little $\Delta C_{p(excess)}$ in this residue. These contrasting properties clearly demonstrate that context is key; the local environment of a positive charge dictates how it contributes to the thermodynamics of unfolding.

On the other hand, the hydrogen bonding of E4 in folded **2** appears itself to be a heat-reservoir, and unfolding leads to a distinct loss of heat capacity. This loss is evidently larger than any loss due to solvation changes, resulting in a negative $\Delta C_{p(excess)}$. However, more examples of peptides containing glutamic and aspartic acid residues are required to solidify or modify this concept.

In general, we attribute the $\Delta C_{p(excess)}$ demonstrated by all residues to the NCIs between them; including those between the mainchain atoms. Nevertheless, there are many open questions regarding the data in Fig. 5. For example, what is the cause of the relatively large positive $\Delta C_{p(excess)}$ values for N6 and Q12? Are the values reported by N6 rooted in the tightness of the turn? Modeling suggests that the relatively large positive $\Delta C_{p(excess)}$ value reported by Q12 is in part rooted to the hydrogen bonding between its sidechain and the sidechain of R1, and its packing to adjacent V3 and I10 (see Section 2.5 of the ESI†), but more is needed here to confirm this. Also, is the increase in $\Delta C_{p(excess)}$ values for G7 in folded **3** and **4** rooted in a decreased solvation of the residue induced by respectively the methyl T4 in **3** and the KMe_3 group in **4**?

Studies of cold denaturation are facilitated by high T_{max} values, and the entropy and heat capacity data obtained here allows us to come to some intriguing conclusions that we have not noted to have been previously articulated. First, because turn residues are more solvent exposed, their changes in heat capacity upon unfolding are generally small. This inevitably contributes to lowering $T_{max(L)}$ values. Moreover, when mutation increases the extent of folding, there is an inevitable increase in order in the turn residues. This also tends to lower $T_{max(L)}$ values. Thus, in general turn residues have intrinsically lower $T_{max(L)}$ values relative to those in sheet structure, and enhanced folding exacerbates this difference. Finally, from the limited set of data thus far gathered a key design principal that can counter the low intrinsic $T_{max(L)}$ values for turn residues is to introduce hydrophobicity near to or at the turn. These lead to less well solvated turn residues that display larger $\Delta C_{p(excess)}$ values. Regardless, the combination of entropy and heat capacity changes at a turn means that a thermodynamic signature of this type of secondary structure are low intrinsic $T_{max(L)}$ values.

Returning to the second question of how local data relates to the global data typically measured, simply averaging the local (L) values give global averages that are reasonable, and sometimes very close to the value obtained by the global (G) assessment using the G7 methylene splitting (see Table 1 and Section 4.4 of the ESI†). However, we believe that a better understanding of the relationship between local and global thermodynamic data requires more peptides and statistical analysis.

Conclusions

We have examined the unfolding of β-hairpin peptides using each mainchain amide as a local reporter. This provides a wealth of thermodynamic data that can be linked to structural elements such as the NCIs that occur between residues. Thus, the four peptides discussed here suggest that a thermodynamic signature of the cation–π interaction is an extremely high $\Delta C_{p(excess)}$ of unfolding. Our work here also suggests that hydrogen bonding carboxylic acids may be heat reservoirs. Finally, the results described here demonstrate that turn residues have intrinsically low $T_{max(L)}$ values, which presumably contribute to reducing the globally assessed $T_{max(G)}$ value of a folded peptide. This suggests that proteins with fewer turns will tend to exhibit higher $T_{max(G)}$ values. We are carrying out further studies to reveal more about how specific residues, secondary structure type, and NCI contribute to fold stability and the phenomenon of cold denaturation. We will report these findings in due course.

Data availability

The data that support the findings of this study are available in the ESI† of the article.

Author contributions

THT performed the complete analysis of peptides **1**, **3** and **4**. PP carried out the complete analysis of peptide **2**. MR and CRT performed the synthesis of peptides **1**–**7**. MLW oversaw the peptide synthesis and provided insight into β-hairpin design. BCG designed the overall study and advised THT and PP.

Conflicts of interest

There are no conflicts to declare.

Acknowledgements

TT and BCG wishes to express their sincere gratitude to the National Institutes of Health for financial support of this work (GM 125690). This work was funded in part by the National Institute of General Medical Sciences of the NIH under award number R35 GM145227 to M. L. W. The NMR data was collected on a 700 MHz NMR spectrometer funded by NSF Major Research Instrumentation Program under the award number DBI-2019046.

References

1 *Biopharmaceutical Market Share Analysis Report by Product Type – Global Industry Demand Forecast to 2030*, Prescient and Strategic Intelligence, 2022, **https://www.psmarketresearch.com/market-analysis/biopharmaceuticals-market**.

2 *Global Biopharmaceutical Stability Testing Market Size*, Global Market Estimates, **https://www.globenewswire.com/en/news-release/2022/08/04/2492452/0/en/Global-Biopharmaceutical-Stability-Testing-Market-Size.html**.

3 P. L. Privalov, Cold denaturation of proteins, *Crit. Rev. Biochem. Mol. Biol.*, 1990, **25**(4), 281–305, DOI: **10.3109/10409239009090612**.

4 F. Franks, Protein Destabilization at Low Temperatures, in *Advances in Protein Chemistry*, ed. C. B. Anfinsen, F. M. Richards, J. T. Edsall and D. S. Eisenberg, Academic Press, 1995, vol. 46, pp. 105–139.

5 W. Blokzijl and J. B. F. N. Engberts, Hydrophobic Effects. Opinions and Facts, *Angew. Chem., Int. Ed.*, 1993, **32**, 1545–1579.

6 S. B. Kim, J. C. Palmer and P. G. Debenedetti, Computational investigation of cold denaturation in the Trp-cage miniprotein, *Proc. Natl. Acad. Sci. U. S. A.*, 2016, **113**(32), 8991–8996, DOI: **10.1073/pnas.1607500113**.

7 K. A. Dill, D. O. V. Alonso and K. Hutchinson, Thermal stabilities of globular proteins, *Biochemistry*, 1989, **28**(13), 5439–5449, DOI: **10.1021/bi00439a019**.

8 C. L. Dias, T. Ala-Nissila, J. Wong-ekkabut, I. Vattulainen, M. Grant and M. Karttunen, The hydrophobic effect and its role in cold denaturation, *Cryobiology*, 2010, **60**(1), 91–99, DOI: **10.1016/j.cryobiol.2009.07.005**.

9 F. Franks, R. H. M. Hatley and H. L. Friedman, The thermodynamics of protein stability: cold destabilization as a general phenomenon, *Biophys. Chem.*, 1988, **31**(3), 307–315, DOI: **10.1016/0301-4622(88)80037-1**.

10 N. V. Prabhu and K. A. Sharp, Heat capacity in proteins, *Annu. Rev. Phys. Chem.*, 2005, **56**, 521–548, DOI: **10.1146/annurev.physchem.56.092503.141202**.

11 C. F. Lopez, R. K. Darst and P. J. Rossky, Mechanistic elements of protein cold denaturation, *J. Phys. Chem. B*, 2008, **112**(19), 5961–5967, DOI: **10.1021/jp075928t**.

12 S. Garde, G. Hummer, A. E. García, M. E. Paulaitis and L. R. Pratt, Origin of Entropy Convergence in Hydrophobic Hydration and Protein Folding, *Phys. Rev. Lett.*, 1996, **77**(24), 4966–4968, DOI: **10.1103/PhysRevLett.77.4966**.

13 D. Sanfelice, R. Puglisi, S. R. Martin, L. Di Bari, A. Pastore and P. A. Temussi, Yeast Frataxin is Stabilized by Low Salt Concentrations: Cold Denaturation Disentangles Ionic Strength Effects from Specific Interactions, *PLoS One*, 2014, **9**(5), e95801, DOI: **10.1371/journal.pone.0095801**.

14 R. Yan, P. DeLos Rios, A. Pastore and P. A. Temussi, The cold denaturation of IscU highlights structure–function dualism in marginally stable proteins, *Commun. Chem.*, 2018, **1**(1), 13, DOI: **10.1038/s42004-018-0015-1**.

15 A. Bitonti, R. Puglisi, M. Meli, S. R. Martin, G. Colombo, P. A. Temussi and A. Pastore, Recipes for Inducing Cold Denaturation in an Otherwise Stable Protein, *J. Am. Chem. Soc.*, 2022, **144**(16), 7198–7207, DOI: **10.1021/jacs.1c13355**.

16 C.-J. Tsai, J. V. Maizel and R. Nussinov, The Hydrophobic Effect: A New Insight from Cold Denaturation and a Two-State Water Structure, *Crit. Rev. Biochem. Mol. Biol.*, 2002, **37**(2), 55–69, DOI: **10.1080/10409230290771456**.

17 Y. V. Griko, P. L. Privalov, J. M. Sturtevant and S. Venyaminov, Cold denaturation of staphylococcal nuclease, *Proc. Natl. Acad. Sci. U. S. A.*, 1988, **85**(10), 3343–3347, DOI: **10.1073/pnas.85.10.3343**.

18 R. Kitahara, A. Okuno, M. Kato, Y. Taniguchi, S. Yokoyama and K. Akasaka, Cold denaturation of ubiquitin at high pressure, *Magn. Reson. Chem.*, 2006, **44**(S1), S108–S113, DOI: **10.1002/mrc.1820**.

19 W. D. Van Horn, A. K. Simorellis and P. F. Flynn, Low-temperature studies of encapsulated proteins, *J. Am. Chem. Soc.*, 2005, **127**(39), 13553–13560, DOI: **10.1021/ja052805i**.

20 J. Seelig and A. Seelig, Protein Stability-Analysis of Heat and Cold Denaturation without and with Unfolding Models, *J. Phys. Chem. B*, 2023, **127**(15), 3352–3363, DOI: **10.1021/acs.jpcb.3c00882**.

21 C. R. Babu, V. J. Hilser and A. J. Wand, Direct access to the cooperative substructure of proteins and the protein ensemble *via* cold denaturation, *Nat. Struct. Mol. Biol.*, 2004, **11**(4), 352–357, DOI: **10.1038/nsmb739**.

22 E. Freire, K. P. Murphy, J. M. Sanchez-Ruiz, M. L. Galisteo and P. L. Privalov, The molecular basis of cooperativity in protein folding. Thermodynamic dissection of interdomain interactions in phosphoglycerate kinase, *Biochemistry*, 1992, **31**(1), 250–256, DOI: **10.1021/bi00116a034**.

23 Y. V. Griko, S. Y. Venyaminov and P. L. Privalov, Heat and cold denaturation of phosphoglycerate kinase (interaction of domains), *FEBS Lett.*, 1989, **244**(2), 276–278, DOI: **10.1016/0014-5793(89)80544-7**.

24 S. T. Whitten, A. J. Kurtz, M. S. Pometun, A. J. Wand and V. J. Hilser, Revealing the Nature of the Native State Ensemble through Cold Denaturation, *Biochemistry*, 2006, **45**(34), 10163–10174, DOI: 10.1021/bi060855+.

25 A. Arsiccio, J. McCarty, R. Pisano and J.-E. Shea, Heightened Cold-Denaturation of Proteins at the Ice–Water Interface, *J. Am. Chem. Soc.*, 2020, **142**(12), 5722–5730, DOI: 10.1021/jacs.9b13454.

26 An interactive graphing 'widget' that allows the user to plot the function $\Delta G(T)$ for various values of ΔC_p, ΔH, and ΔS is provided in Section 4.3.2 of the ESI.†

27 P. L. Privalov, E. I. Tiktopulo, S. Y. Venyaminov, Y. V. Griko, G. I. Makhatadze and N. N. Khechinashvili, Heat capacity and conformation of proteins in the denatured state, *J. Mol. Biol.*, 1989, **205**(4), 737–750, DOI: 10.1016/0022-2836(89)90318-5.

28 R. L. Baldwin, Gas-liquid transfer data used to analyze hydrophobic hydration and find the nature of the Kauzmann-Tanford hydrophobic factor, *Proc. Natl. Acad. Sci. U. S. A.*, 2012, **109**(19), 7310–7313, DOI: 10.1073/pnas.1203720109.

29 K. P. Murphy, P. L. Privalov and S. J. Gill, Common Features of Protein Unfolding and Dissolution of Hydrophobic Compounds, *Science*, 1990, **247**(4942), 559–561, DOI: 10.1126/science.2300815.

30 K. P. Murphy and S. J. Gill, Solid Model Compounds and the Thermodynamics of Protein Unfolding, *J. Mol. Biol.*, 1991, **222**, 699–709.

31 K. P. Murphy and S. J. Gill, Group additivity thermodynamics for dissolution of solid cyclic dipeptides into water, *Thermochim. Acta*, 1990, **172**, 11–20, DOI: 10.1016/0040-6031(90)80555-D.

32 R. L. Baldwin, Temperature dependence of the hydrophobic interaction in protein folding, *Proc. Natl. Acad. Sci. U. S. A.*, 1986, **83**, 8069–8072.

33 A. D. Robertson and K. P. Murphy, Protein Structure and the Energetics of Protein Stability, *Chem. Rev.*, 1997, **97**, 1251–1267.

34 G. I. Makhatadze, M. M. Lopez and P. L. Privalov, Heat capacities of protein functional groups, *Biophys. Chem.*, 1997, **64**(1), 93–101, DOI: 10.1016/S0301-4622(96)02234-X.

35 P. L. Privalov and G. I. Makhatadze, Contribution of Hydration to Protein Folding Thermodynamics: II. The Entropy and Gibbs Energy of Hydration, *J. Mol. Biol.*, 1993, **232**(2), 660–679, DOI: 10.1006/jmbi.1993.1417.

36 R. M. Hughes and M. L. Waters, Arginine methylation in a β-hairpin peptide: implications for Arg-π interactions, ΔC_p, and the cold denatured state, *J. Am. Chem. Soc.*, 2006, **128**(39), 12735–12742, DOI: 10.1021/ja061656g.

37 C. D. Tatko and M. L. Waters, Comparison of C-H···π and hydrophobic interactions in a β-hairpin peptide: impact on stability and specificity, *J. Am. Chem. Soc.*, 2004, **126**(7), 2028–2034, DOI: 10.1021/ja038258n.

38 R. M. Hughes, K. R. Wiggins, S. Khorasanizadeh and M. L. Waters, Recognition of trimethyllysine by a chromodomain is not driven by the hydrophobic effect, *Proc. Natl. Acad. Sci. U. S. A.*, 2007, **104**(27), 11184–11188, DOI: 10.1073/pnas.0610850104.

39 G. S. Buchner, N. Shih, A. E. Reece, S. Niebling and J. Kubelka, Unusual Cold Denaturation of a Small Protein Domain, *Biochemistry*, 2012, **51**(33), 6496–6498, DOI: 10.1021/bi300916v.

40 F. Franks and R. H. M. Hatley, Low-temperature unfolding of chymotrypsinogen, *Cryobiology*, 1985, **22**(6), 608, DOI: 10.1016/0011-2240(85)90058-6.

41 R. H. M. Hatley and F. Franks, Cold destabilisation of enzymes, *Faraday Discuss.*, 1992, **93**, 249–257, DOI: 10.1039/FD9929300249.

42 M. Davidovic, C. Mattea, J. Qvist and B. Halle, Protein Cold Denaturation as Seen From the Solvent, *J. Am. Chem. Soc.*, 2009, **131**(3), 1025–1036, DOI: 10.1021/ja8056419.

43 D. A. Stauffer, R. E. Barrans and D. A. Dougherty, Concerning the Thermodynamics of Molecular Recognition in Aqueous and Organic Media – Evidence for Significant Heat-Capacity Effects, *J. Org. Chem.*, 1990, **55**(9), 2762–2767, DOI: 10.1021/Jo00296a038.

44 R. B. Dyer, S. J. Maness, S. Franzen, R. M. Fesinmeyer, K. A. Olsen and N. H. Andersen, Hairpin Folding Dynamics: The Cold-Denatured State is Predisposed for Rapid Refolding, *Biochemistry*, 2005, **44**(30), 10406–10415, DOI: 10.1021/bi050698z.

45 N. H. Andersen, J. R. Cort, Z. Liu, S. J. Sjoberg and H. Tong, Cold Denaturation of Monomeric Peptide Helices, *J. Am. Chem. Soc.*, 1996, **118**, 10309–10310.

46 J. Sabelko, J. Ervin and M. Gruebele, Cold-Denatured Ensemble of Apomyoglobin: Implications for the Early Steps of Folding, *J. Phys. Chem. B*, 1998, **102**(10), 1806–1819, DOI: 10.1021/jp973178p.

47 K.-B. Wong, S. M. V. Freund and A. R. Fersht, Cold Denaturation of Barstar: ^{1}H, ^{15}N and ^{13}C NMR Assignment and Characterisation of Residual Structure, *J. Mol. Biol.*, 1996, **259**(4), 805–818, DOI: 10.1006/jmbi.1996.0359.

48 J. Jonas, L. Ballard and D. Nash, High-resolution, high-pressure NMR studies of proteins, *Biophys. J.*, 1998, **75**(1), 445–452, DOI: 10.1016/S0006-3495(98)77532-0, acccessed 2023/07/25.

49 J. Jonas, High-resolution nuclear magnetic resonance studies of proteins, *Biochim. Biophys. Acta*, 2002, **1595**(1), 145–159, DOI: 10.1016/S0167-4838(01)00341-7.

50 F. A. Syud, J. F. Espinosa and S. H. Gellman, NMR-Based Quantification of β-Sheet Populations in Aqueous Solution through Use of Reference Peptides for the Folded and Unfolded States, *J. Am. Chem. Soc.*, 1999, **121**(49), 11577–11578, DOI: 10.1021/ja992733t.

51 H. E. Stanger and S. H. Gellman, Rules for Antiparallel β-Sheet Design: D-Pro-Gly is Superior to L-Asn-Gly for β-Hairpin Nucleation, *J. Am. Chem. Soc.*, 1998, **120**(17), 4236–4237, DOI: 10.1021/ja973704q.

52 F. A. Syud, H. E. Stanger and S. H. Gellman, Interstrand Side Chain-Side Chain Interactions in a Designed β-Hairpin: Significance of Both Lateral and Diagonal Pairings, *J. Am. Chem. Soc.*, 2001, **123**, 8667–8677.

53 R. M. Hughes, M. L. Benshoff and M. L. Waters, Effects of chain length and *N*-methylation on a cation-π interaction in a β-hairpin peptide, *Chemistry*, 2007, **13**(20), 5753–5764, DOI: **10.1002/chem.200601753**.

54 R. M. Hughes, K. R. Wiggins, S. Khorasanizadeh and M. L. Waters, Recognition of trimethyllysine by a chromodomain is not driven by the hydrophobic effect, *Proc. Natl. Acad. Sci. U. S. A.*, 2007, **104**(27), 11184–11188, DOI: **10.1073/pnas.0610850104**.

55 R. M. Hughes and M. L. Waters, Influence of *N*-methylation on a cation-π interaction produces a remarkably stable β-hairpin peptide, *J. Am. Chem. Soc.*, 2005, **127**(18), 6518–6519, DOI: **10.1021/ja0507259**.

56 E. G. Hutchinson and J. M. Thornton, A revised set of potentials for β-turn formation in proteins, *Protein Sci.*, 1994, **3**(12), 2207–2216, DOI: **10.1002/pro.5560031206**.

57 S. R. Griffiths-Jones, A. J. Maynard, G. J. Sharman and M. S. Searle, NMR evidence for the nucleation of a β-hairpin peptide conformation in water by an Asn-Gly type I′ β-turn sequence, *Chem. Commun.*, 1998, (7), 789–790, DOI: **10.1039/A800749G**.

58 A. J. Maynard, G. J. Sharman and M. S. Searle, Origin of β-Hairpin Stability in Solution: Structural and Thermodynamic Analysis of the Folding of a Model Peptide Supports Hydrophobic Stabilization in Water, *J. Am. Chem. Soc.*, 1998, **120**(9), 1996–2007, DOI: **10.1021/ja9726769**.

59 In such analyses, error propagation (see Appendix 1 of ESI†) reveals sizable errors for poorly or highly folded peptides, and minimal errors for intermediately folded hairpins. Specifically, the maximum error in ΔG_u is greater than 33% if $f > 0.9$ or $f < 0.1$, ranges from 14% to 33% if $0.1 < f < 0.3$ or $0.7 < f < 0.9$, and ranges from 12% to 14% if $0.3 < f < 0.7$.

60 M. S. Searle, S. R. Griffiths-Jones and H. Skinner-Smith, Energetics of Weak Interactions in a β-Hairpin Peptide: Electrostatic and Hydrophobic Contributions to Stability from Lysine Salt Bridges, *J. Am. Chem. Soc.*, 1999, **121**(50), 11615–11620, DOI: **10.1021/ja992029c**.

61 Select studies at pH = 5.6 (sodium acetate buffer) led to essentially the same results as those described.

62 Note that although the K9KMe$_3$ mutation does not result in non-monotonicity in the X9 amide signal, this mutation does result in significant difference to the $\Delta\delta(T)$ function of the sidechain methylenes of the X9 residue. (See Section 6, ESI†).

63 Two amide signals, those of R1 and L11, were not amenable to this analysis because of signal overlap with the corresponding 6-mer half peptides (Section 4.3 of the ESI†).

64 Note that the NOEs associated with X4 in peptides **1** and **2** are indistinguishable.

65 G. I. Makhatadze and P. L. Privalov, Heat capacity of proteins: I. Partial molar heat capacity of individual amino acid residues in aqueous solution: hydration effect, *J. Mol. Biol.*, 1990, **213**(2), 375–384, DOI: **10.1016/S0022-2836(05)80197-4**.

66 The sidechain of a folded protein is understood to contribute less than 10% of the total heat capacity change upon unfolding.

67 This $\Delta C_{p(L)}$ difference is not in itself within error, so the calculated $\Delta T_{max(L)}$ may be anomalously high.

68 The insignificant change in $\Delta C_{p(L)}$ at O8 leads to large error because of the near linearity of the $\Delta G(T)$ function. This error is also apparent in the calculated $T_{max(L)}$ data.

69 N. K. Pinkin and M. L. Waters, Development and mechanistic studies of an optimized receptor for trimethyllysine using iterative redesign by dynamic combinatorial chemistry, *Org. Biomol. Chem.*, 2014, **12**(36), 7059–7067, DOI: **10.1039/c4ob01249f**.

70 L. A. Ingerman, M. E. Cuellar and M. L. Waters, A small molecule receptor that selectively recognizes trimethyl lysine in a histone peptide with native protein-like affinity, *Chem. Commun.*, 2010, **46**(11), 1839–1841, DOI: **10.1039/C000255K**.

71 K. D. Daze and F. Hof, The cation-π interaction at protein-protein interaction interfaces: developing and learning from synthetic mimics of proteins that bind methylated lysines, *Acc. Chem. Res.*, 2013, **46**(4), 937–945, DOI: **10.1021/ar300072g**.

72 T. Jenuwein and C. D. Allis, Translating the histone code, *Science*, 2001, **293**(5532), 1074–1080, DOI: **10.1126/science.1063127**.

73 R. E. McGovern, B. D. Snarr, J. A. Lyons, J. McFarlane, A. L. Whiting, I. Paci, F. Hof and P. B. Crowley, Structural study of a small molecule receptor bound to dimethyllysine in lysozyme, *Chem. Sci.*, 2015, **6**(1), 442–449, DOI: **10.1039/C4SC02383H**.